Physical mechanisms driving the global ocean breathing

Esther Portela[1]*, Nicolas Kolodziejczyk[1], Virginie Thierry[1] and Clément Vic[1]

[1]Univ. Brest, CNRS, IRD, Ifremer, Laboratoire d'Oceanographie Physique et Spatiale (LOPS), Plouzane, France

Key Points:

- Up to 70% of the global oxygen uptake occurs during Mode Water subduction,driven by lateral induction and vertical velocity.
- Oxygen diffusion, despite large uncertainties, is likely to play an important role in the global oxygen uptake.
- Total oxygen subduction is driven by the mass flux, with little contribution of the latitudinal variability of the $[O_2]$.

Corresponding author: Esther Portela, eportelanh@gmail.com

Abstract

Future changes in subduction are suspected to be critical for the ocean deoxygenation predicted by climate models over the 21^{st} century. However, the drivers of global oxygen subduction have not been fully described or quantified. Here, we address the physical mechanisms responsible for the oxygen transport across the late winter mixed layer base and their relation with water-mass formation. Up to 70% of the global oxygen uptake takes place during Mode Water subduction mostly in the Southern Ocean and the North Atlantic. This oxygen subduction is driven by the combination of strong currents with large mixed-layer-depth gradients at localized hot-spots and by the wind-driven vertical velocity within the Subtropical gyres. Although oxygen diffusion, often neglected, is uncertain, it is likely to be important for the global oxygenation. The physical mass flux dominates the total oxygen subduction while the oxygen solubility plays a minor role in its modulation.

1 Introduction

A global ocean deoxygenation trend has been observed over the past decades and it is predicted by climate models to increase over this century (Helm et al., 2011; Schmidtko et al., 2017; Keeling & Garcia, 2002; Keeling et al., 2010; Ito et al., 2017; Oschlies et al., 2018; Bopp et al., 2002, 2013). This decrease in the global ocean oxygen concentration ($[O_2]$) has been attributed to the warming climate operating directly via the decrease of oxygen solubility and indirectly by an increased stratification and changes in respiration and ventilation (Oschlies et al., 2018; Schmidtko et al., 2017). Ocean ventilation refers to the combination of processes by which the surface waters that have been recently in contact with the atmosphere are injected into the ocean interior (like kinematic and diffusive subduction) (Cushman-Roisin, 1987; Qiu & Huang, 1995; Marshall et al., 1993) and transported away from their sources (interior circulation and mixing) (Naveira Garabato et al., 2017; Luyten et al., 1983).

Reduced ventilation has been proposed as the main mechanism driving the ongoing global oxygen loss (Helm et al., 2011; Keeling et al., 2010; Keeling & Garcia, 2002; Long et al., 2016). However, the different ventilation processes have not been fully unraveled or quantified. On decadal timescales, the strongest negative oxygen trends have been detected in the least ventilated regions with an associated expansion of the oxygen minimum zones (Stramma et al., 2008; Schmidtko et al., 2017; Helm et al., 2011), while newly subducted water masses do not show a detectable deoxygenation signal (Oschlies et al., 2018; Schmidtko et al., 2017; Helm et al., 2011). These patterns suggest that oxygen loss over the past decades is consistent with a reduced interior transport and the overturning circulation slowdown (Schmidtko et al., 2017; Brandt et al., 2015; Oschlies et al., 2018). In contrast, a recent climate model simulation has shown a major contribution of a reduced subduction to the long-term oxygen loss, suggesting that changes in location and intensity of subduction are critical to understand the long-term deoxygenation (Couespel et al., 2019).

Oxygen can be brought into the ocean interior through water mass formation at high latitudes and released back into the mixed layer (ML) in zones of strong upwelling (Liu & Huang, 2012). However, the mechanisms setting the relationship between these ventilation regions and the associated water masses are still poorly understood at global scales.

In the context of climate change, given the importance of the subduction process for the present and future of the oceanic oxygen content, it is crucial to understand and quantify the global oxygen subduction (S^{ox}). We focus on the relative contribution of the physical mechanisms driving the oxygen uptake and release by the interior ocean, i.e. the global ocean breathing.

2 Key concepts on oxygen subduction

There are three competing processes driving the global ocean oxygen inventory: (i) the air/sea transfer tied to oxygen solubility (Koelling et al., 2017), mainly controlled by the seawater temperature, (ii) the S^{ox} that carries the oxygen-rich surface waters to the ocean interior (Cushman-Roisin, 1987; Marshall et al., 1993) and (iii) the biological respiration and remineralization (Resplandy, 2018; Wyrtki, 1965). Within the ML, $[O_2]$ is, to first order, in equilibrium with the atmosphere and therefore close to 100% saturation (O_{sat}), deviations from saturation are usually found in deep convection zones (Koelling et al., 2017).

In Figure 1 we illustrate the oxygen subduction/obduction process and their effect on the interior $[O_2]$ ($[O_2]_i$) and oxygen inventory. The ML is considered as a buffer between the atmosphere and the ocean interior. Oxygen obduction (O^{ox}) is defined here as the opposite of subduction, i.e. the oxygen flux from the permanent thermocline through the steady, late winter ML base into the seasonal thermocline/ML (Sallée et al., 2012, 2010; Marshall et al., 1993; Kwon et al., 2016). To isolate the subduction effect, for simplicity, in this conceptual schematic we set a steady oxygen solubility in the ML and a constant respiration in time and space. While biogeochemical processes are important to modulate the $[O_2]$ in certain regions (Richardson & Bendtsen, 2017), they are beyond the scope of this study.

Putting aside the effect of biogeochemical processes, the S^{ox} increases the oxygen inventory within a given volume delimited by the late winter ML base and an isopycnal surface (σ_n). This is due to the volume augmentation and to the uptake of well oxygenated waters with $[O_2] \approx O_{sat}$ by the interior ocean. Since O_{sat} is usually higher than $[O_2]_i$, this process also increases $[O_2]_i$.

In an obductive location, the oxygen inventory decreases due to a negative mass flux. However, this flux alone will not change the $[O_2]$ of the given volume ($\Delta[O_2]_i = 0$, Figure 1b). In the ML, the $[O_2]$ ($[O_2]_{ml}$) decreases due to the mixing of nearly saturated with interior, less oxygenated waters. However, due to the air-sea equilibrium, the $[O_2]_{ml}$ rapidly re-saturates (few days for a ML of 50 m (Gruber et al., 2001)). Note that oxygen diffusion can take place in a net obductive location where it would increase the local $[O_2]_i$. However, the kinematic mass and oxygen flux to the mixed layer would overwhelm this effect. As in the global ocean mass must be conserved, the obduction and subduction mass flux must compensate each other. This implies that S^{ox} is the only dynamical mechanism able to increase the global $[O_2]_i$. The subsequent water-mass mixing and spreading do not change the global oxygen inventory, but they drive the oxygen distribution over the entire ocean at interannual to decadal timescales (Joos et al., 2003).

3 Methods

3.1 Oxygen Subduction Computation

While the ML depth varies seasonally with the resulting entrainment/detrainment of water, permanent subduction (in contrast with the instantaneous subduction first described by Cushman-Roisin (1987)) accounts for the fraction of water that has irreversibly entered the permanent thermocline across the steady late-winter ML base (H_{max}) (Donners et al., 2005; Marshall et al., 1993). This permanent S^{ox} is determined by the mass flux across H_{max} carrying the measured oxygen (kinematic subduction) and by the turbulent oxygen diffusion due to the difference in $[O_2]$ in the ML/seasonal thermocline and the ocean interior. Its net value (positive into the ocean interior and negative into the thermocline) is the sum of the contributing terms that are expressed as follows (Sallée et al., 2012):

$$\overline{S^{ox}} = \underbrace{\overline{[O_2]} \cdot \overline{U} \cdot \nabla_h \overline{H_{max}}}_{\text{Lateral induction}} + \underbrace{\overline{[O_2]} \cdot \nabla_h (\overline{U^* H_{max}})}_{\text{Eddy-induced}} + \underbrace{\overline{[O_2]} \cdot \overline{w}}_{\text{Vertical}} + \underbrace{k_v \cdot \nabla_v \overline{[O_2]_h} + k_h \cdot \nabla_h \overline{[O_2]_h} \cdot \nabla_h \overline{H_{max}}}_{\text{Diffusion}} \tag{1}$$

Where U and U^* are respectively the horizontal mean and bolus velocity fields, w is the vertical velocity and ∇_h is the horizontal divergence operator. U^*, represents the advective contribution of unresolved eddies (Forget et al., 2015) parametrized following (Gent & McWilliams, James, 1990). Vertical diffusion in the ocean interior is mainly driven by turbulent mixing induced by the breaking of internal tides (Munk & Wunsch, 1998). Hence, we use a geographically-variable vertical diffusion coefficient k_v based on a parametrisation of tidally-driven mixing (de Lavergne et al., 2020). k_v is determined at the base of the mixed layer as $k_v = 0.2\varepsilon/N^2$ (Osborn, 1980), where ε is the turbulent energy dissipation and N^2 is the buoyancy frequency.

Based on previous studies, the lateral diffusion coefficient is set to be $k_h = 10^3 m^2 s^{-1}$ (Köhl et al., 2007; Forget et al., 2015) but this coefficient is spatially variable (Klocker & Abernathey, 2014; Abernathey & Marshall, 2013) and uncertain as it is based in parametrisations that depend on the dataset resolution. To discuss the potential role of diffusion on the global oxygen uptake we have computed it with the lower and higher k_h boundaries ($k_h = 10^2 - 10^4 m^2 s^{-1}$, (Forget et al., 2015)). Here, we examine mean S^{ox} from monthly climatological fields (overbars in 1) and the resulting mean S^{ox} is the average of the monthly fields.

Following Sallée et al. (2010), S^{ox} was computed by considering that $H_{max} = H_{ml} + H_{sth}$, where subscripts ml and sth denote the seasonal ML and the seasonal thermocline respectively (Figure 1). Since H_{max} is fixed over the annual cycle, the decomposition of the lateral induction term in Eq. 1 (similarly applied to the eddy-induced term) becomes:

$$\overline{[O_2]} \cdot \overline{U} \cdot \nabla_h \overline{H} = \overline{[O_2]}_{ml} \cdot \overline{U_{ml}} \cdot \nabla_h \overline{H_{ml}} + \overline{[O_2]}_{sth} \cdot \overline{U_{sth}} \cdot \nabla_h \overline{H_{sth}} \tag{2}$$

This method takes into account the seasonal variation of the surface $[O_2]$ and the different U and U^* in the two layers whose respective thickness vary seasonally. In the case of obduction, we considered the $[O_2]$ below the deepest ML base. The uncertainty associated with the sparse oxygen sampling and the interannual variability of oxygen and subduction is discussed in the supplementary material (Figures S3, S4).

3.2 Data

All the physical variables were obtained from the reanalysis produced by the consortium for Estimating the Circulation and Climate of the Ocean (ECCOv4 r3) (Fukumori et al., 2017). We have used climatological monthly mean values averaged over 1992-2015 with horizontal resolution of 0.5°x0.5°. The vertical grid spacing increases from 10 m near the surface to 457 m near the ocean bottom.

To validate the results obtained with ECCOv4, we computed the kinematic S^{ox} using the gridded Argo product "In situ Analysis System" (ISAS15) (Gaillard et al., 2016; Kolodziejczyk et al., 2017). The resulting fields are available in the supporting information and show a good agreement (Figure S2).

The monthly climatological dissolved oxygen data were obtained from the World Ocean Atlas 2018 (WOA18) (Garcia et al., 2019), which provides statistical and objectively analysed data fields at 1°x1° resolution. All measurements used in this database have been obtained through the Winkler titration method. The oxygen field was then interpolated onto the ECCOv4 grid. The WOA18 climatology contains data from 1955 to 2017. The different time window used to compute WOA18 and ECCOv4 climatologies constitutes a source of uncertainty.

4 Results

4.1 Geographical distribution of oxygen subduction

The largest oxygen fluxes into the thermocline are located (i) in the Southern Ocean (37%), with maximum to the east of Drake Passage and (ii) in the northern North Atlantic (30%), particularly in Labrador, Irminger and Nordic Seas (Liu & Huang, 2012). The Barents Sea constitutes an isolated hot-spot of oxygen uptake (Figure 2e) within the Arctic Ocean. In addition, we can identify weaker, but homogeneous subductive regions shaped by the subtropical gyres in every ocean basin. The majority of the O^{ox} occurs in three regions: around 45% takes place in the Southern Ocean, around 22% in the subtropical-subpolar North Atlantic and 14% in the equatorial strip.

The S^{ox} is globally shaped by the lateral induction (Figure 2a), the component with the highest magnitude located in well defined hot-spots. Nonetheless it produces a global net deoxygenation (-142 $Tmol\ yr^{-1}$). Lateral induction is driven by large MLD gradients in combination with strong regional currents (Figure S1b). It is maximum in the northern North Atlantic (Labrador and Irminger and Nordic seas) and in the Southern Ocean. The latter, driven by intense Antarctic Circumpolar Current (ACC) (Figure S1b). In the subtropical-subpolar North Atlantic, the Gulf Stream and the North Atlantic Current act as dynamical barriers; weak oxygen uptake occurs to the southeast, while intense O^{ox} extends northeastward from the Florida Strait to the Norwegian Seas (Figure 2d)(Marshall et al., 1993; Qiu & Huang, 1995).

The eddy-induced term (Figure 2b), plays a role in the S^{ox}, especially in the North Atlantic and the Southern Ocean (Sallée et al., 2010; Portela et al., 2020). However, the main contributor to the ocean oxygenation is the vertical velocity (299 $Tmol\ yr^{-1}$). This term is relatively weak but homogeneously positive over the large extension of the subtropical gyres. Nonetheless, negative vertical velocity drives O^{ox} near Antarctica and in the equatorial upwelling band where it dominates the total oxygen flux.

Oxygen diffusion, as found in other studies (Sallée et al., 2012; Kwon et al., 2016), is one order of magnitude smaller than the other terms at regional scale, but it is not negligible in the global integral. Diffusion estimations are uncertain since they are based on parametrisations. However, its vertical component is well represented in this study and, depending on the value of the lateral component, diffusion might be a key process for the ocean oxygenation. The vertical and lateral oxygen diffusion are shown separately in Figure S6 (supporting information).

To first order, mass and properties subducted into the ocean interior spread along isopycnals and the $[O_2]$ diminishes by mixing and biological consumption along the spreading path. The analysis of Apparent Oxygen Utilization (AOU= $O_{sat} - [O_2]$) sections across every ocean basin (Figure 3) can be seen as a proxy of the water-mass age (a reasonable assumption around the ML base (Brandt et al., 2015)) and it can trace back the main ventilation hot-spots in a way similar to the Lagangian approach.

Most obductive regions show relatively high AOU (Figure 3) which indicates that water has been subducted in remote locations and undergone mixing and biological consumption along its path. In the particular case of the North Atlantic, water subducted within the Subpolar Gyre in the Labrador Sea is transported into deep layers (>1000 m) while the water obducted further south, downstream of the main Gyre's flow has a different, less dense, subtropical origin (Figure 3c). However, the resolution of our computations does not allow to elucidate if the oxygen subducted in the Irminger Sea experiences further reventilation and is re-subducted in the Labrador Sea (Figure S5) as suggested by (McCartney, 1982).

In the Indian and Pacific basins, recently subducted waters with low AOU are isopycnally transported and mixed northwards (Figure 3a, b,d). In these basins, Mode Waters (delimited by the two upper thick contours in Figures 3(a-c) are never reventilated, which results in increased AOU along their northward journey.

In the Southern Ocean (Figure 3d), well oxygenated waters are subducted near Antarctica during Bottom Water formation (Speer et al., 2000; Marshall & Speer, 2012). This feature, is not well captured in our S^{ox} computation (Figure 2) but it leaves its signature with a relative deep AOU minimum deeper than 2000 m (Figure 3a-c).

4.2 Water-mass ventilation

The integrated effect of the S^{ox} on isopycnals provides additional insight on the ocean (de)oxygenation during water-mass formation and erosion. As expected, the maximum oxygen uptake in every ocean basin occurs within the Mode Waters density range (Figure 4a-f) (Karstensen et al., 2008). Moreover, while Mode Waters density outcrops occupy 36% of the ML-base surface, they jointly account for 70% of the global oxygen uptake and they are dominant in every ocean basin (Figure 4f).

The intense oxygen uptake during Subantarctic Mode Water (SAMW) subduction occurs over a narrow density range in each Southern Ocean basin (Liu & Huang, 2012; Sallée et al., 2010; Portela et al., 2020).

In the northern North Atlantic, the outcropping isopycnals denser than 26.5 kg m^{-3} undergo wide meridional excursions (Luyten et al., 1985) (Figure 2d). Due to that, the strong S^{ox} detected at σ=27.8 kg m^{-3} comprises both, the Subpolar Mode Water (SPMW) and waters of the Nordic Seas where strong deep convection and associated subduction occurs (Marshall, 1999). Half of the oxygen uptake in the Southern Ocean and the North Atlantic is tied to SAMW and SPMW formation (Figure 4f) which occurs within only 22% and 15% of the global outcropping density surface respectively. Hereinafter we will refer to the ensemble of these two mode waters as Subantarctic-Subpolar Mode Waters (SA-SPMW). This strong oxygen uptake during SA-SPMW formation is driven by lateral induction. The diffusion contribution is negligible with the reference diffusivity considered in this study but it could be important in the SA-SPMW density range with an enhanced k_l value, as shown by the bars contours in Figure 4 (a-e).

The second peak of S^{ox} corresponds to Subtropical Mode Waters (STMW). It is less intense, but extends over a greater density range than SA-SPMW (Figure 4). Particularly in the North Pacific ocean, oxygen subducted during STMW formation accounts for more than half of the oxygen uptake (Figure 4f). The S^{ox} by STMW is driven by the vertical velocity (highlighted in Figure 4g), in majority explained by Ekman pumping (Qiu & Huang, 1995; Marshall et al., 1993).

The maximum O^{ox} occurs (i) in the Southern Ocean, associated with the obduction mass flux that erodes the AAIW (Portela et al., 2020) driven by a combination of lateral induction and wind-driven vertical flux (Figure 4a-c) (ii) in the North Atlantic, driven by lateral induction (Figure 4e and (iii) in the equatorial strip (Figure 2c), where the wind-driven upwelling represents the zonal maximum of oxygen release (Figure 4g).

The spatial distribution of $[O_2]$, with the exception of the equatorial band, has a negligible effect on the global S^{ox} which in turn is determined by the mass flux (Kwon et al., 2016). This is suggested by the small difference between S^{ox} as computed from Eq.1 (filled area in Figure 4g), and that computed by assuming spatially homogeneous $[O_2]$ (black curve).

5 Discussion and Conclusion

The results presented here, show the mean state of the global S^{ox}. This is regulated by the physical mass flux while the spatial distribution of the $[O_2]$ at the ML base, linked to solubility effect, has a minor role (Kwon et al., 2016). In this study we provide a thorough description and the first quantification of the physical drivers of the ocean breathing. SA-SPMW are formed in hot-spots of intense lateral induction, while the wind-driven vertical velocity, although locally weak, dominates STMW subduction within the subtropical gyres. The percentage of oxygen that is globally subducted during mode water formation (70%) almost doubles that of the surface occupied by its outcropping isopycnals (36%) at the ML base. The enhanced contribution of mode water to the oxygen injection into the ocean interior corroborates their key role in ocean oxygenation.

Oxygen diffusion, a term often neglected (Kwon et al., 2016; Sallée et al., 2012) is locally small, but it becomes important in the global integral. The role of tidally-driven mixing in shaping the concentration of passive tracers in the open ocean has recently been highlighted by Tuerena et al. (2019). However, the choice of lateral diffusivity coefficients is largely uncertain and the diffusion contribution to the global oxygen uptake ranges from little to overwhelming. While the k_v computed here is a reliable value, it is likely underestimated since it only considers the tidal mixing and it does not account for convective-driven mixing (Yeager & Large, 2007; Kolodziejczyk & Gaillard, 2013). A negative oxygen diffusion trend was found to be the dominant contributor of the predicted ocean deoxygenation over this century(Couespel et al., 2019). In line with these findings, our results underline the need to improve the global mapping of diffusion to fully understand the mechanisms of the ocean (de)oxygenation.

The Southern Ocean and the North Atlantic are the two lungs of the ocean. One third of the global oxygen uptake and nearly half of the oxygen release take place in the Southern Ocean. Moreover, the inter-basin exchange provided by the ACC is, at least, one order of magnitude larger than all the other inter-basin flows combined (Rintoul, 2000) which increases the potential of the Southern Ocean to provide oxygen to the rest of the ocean. The oxygen subducted in the Southern Ocean is distributed (i) to intermediate depths following SAMW formation (Portela et al., 2020; Kolodziejczyk et al., 2019; Hanawa & Talley, 2001) and (ii) to the deep ocean during the Bottom Water formation (Speer et al., 2000; Marshall & Speer, 2012; Rintoul, 2000). On the other hand, the Northern North Atlantic, following winter deep convection (Wolf et al., 2018; Körtzinger et al., 2004; Fröb et al., 2016), oxygen is provided to Circumpolar Deep Waters as part of the Atlantic Meridional Overturning Circulation (AMOC) (Lumpkin & Speer, 2007).

The strong obduction regions in the Southern Ocean have been substantially affected by deoxygenation over the past decades (Oschlies et al., 2018; Helm et al., 2011). This can be explained by an increase of the obduction rate in the Southern Ocean together with the stratification increase. The resulting reduced ventilation leads to a progressive substitution of relatively oxygenated waters by older waters with lower $[O_2]$ (Helm et al., 2011). This, in addition to the slowdown of the AMOC over the 20^{th} century (Rahmstorf et al., 2015) are consistent with the stronger global deoxygenation of deep waters (>1200 m) in comparison with those of surface and intermediate depths (Oschlies et al., 2018).

In this study, we investigated the S^{ox} as the only physical mechanism leading to the injection of oxygen from the mixed layer into the ocean interior. While it is generally assumed that ocean mixing and air-sea oxygen fluxes prevent the retention of biologically produced oxygen in the ocean, it has been suggested that subsurface primary production makes a contribution to the oxygen flux in permanent stratified regions of the ocean as the Oxygen minimum zones (Richardson & Bendtsen, 2017).

S^{ox} is critical for the long-term oxygen inventory. However, some of its components, like diffusion or eddy-induced subduction, are still uncertain and others, depend on the mixed layer depth, which show large variation between datasets (not shown). Thus, it is of key importance to reduce these uncertainties in order to better understand the global ocean deoxygenation and to improve the model estimations and forecasts. The results presented here provide new insights into the quantification of the physical contributors to the ocean breathing. However, the historical dissolved oxygen dataset is still sparse, and this prevents from obtaining a reliable global oxygen inventory and separating natural variability from long-term climate-related trend. Ongoing deployment of biogeochemical Argo global network including systematic oxygen measurements will bring new opportunities for investigating the global (de)oxygenation drivers and for monitoring the temporal evolution of S^{ox} as well as the biogeochemical processes.

Acknowledgments

This study has been funded by the ACcOLADe LEFE/INSU project and E.P has been supported by a CNES/CNRS/Ifremer post-doctoral grant. The data used in this study are publicly available. ECCOv4 data can be obtained here: https://ecco.jpl.nasa.gov/drive/files. WOD18 oxygen data can be obtained here: https://www.nodc.noaa.gov/OC5/woa18/woa18data.html. ISAS15 is produced at LOPS as part of the Service National d'Observation Argo-France and made is freely available (doi:http://doi.org/10.17882/52367). The vertical diffusivity fields are available at https://www.seanoe.org/data/00619/73082/. We thank D. Couespel for valuable discussions on this subject and H. Regan for the English revision.

6 Author contributions

E.P and N.K conceived the idea of this study. E.P was the main writer of the manuscript and performed the computations with support from N.K. except for the diffusivity which was performed by C.V. All the authors participated in the analysis of the results and the writing of the manuscript in its final form.

References

Abernathey, R. P., & Marshall, J. (2013). Global surface eddy diffusivities derived from satellite altimetry. *Journal of Geophysical Research: Oceans*, *118*(2), 901–916. doi: 10.1002/jgrc.20066

Bopp, L., Le Quéré, C., Heimann, M., Manning, A. C., & Monfray, P. (2002). Climate-induced oceanic oxygen fluxes: Implications for the contemporary carbon budget. *Global Biogeochemical Cycles*, *16*(2), 6–1–6–13. doi: 10.1029/2001gb001445

Bopp, L., Resplandy, L., Orr, J. C., Doney, S. C., Dunne, J. P., Gehlen, M., ... Vichi, M. (2013). Multiple stressors of ocean ecosystems in the 21st century: Projections with CMIP5 models. *Biogeosciences*, *10*(10), 6225–6245. doi: 10.5194/bg-10-6225-2013

Brandt, P., Bange, H. W., Banyte, D., Dengler, M., Didwischus, S. H., Fischer, T., ... Visbeck, M. (2015). On the role of circulation and mixing in the ventilation of oxygen minimum zones with a focus on the eastern tropical North Atlantic. *Biogeosciences*, *12*(2), 489–512. doi: 10.5194/bg-12-489-2015

Couespel, D., Marina, L., & Bopp, L. (2019). Major contribution of reduced upper ocean oxygen mixing to global ocean deoxygenation in an Earth System Model. *Geophysical Research Letters*, 1–23. doi: 10.1029/2019GL084162

Cushman-Roisin. (1987). Subduction. Dynamics of the Oceanic Surface Mixed Layer. In *Proc. 'aha huliko'a hawaiian winter workshop, honolulu, hi, university of hawaii at manoa* (pp. pp. 181–196).

de Lavergne, C., Vic, C., Madec, G., Roquet, F., Waterhouse, A. F., Whalen, C. B., ... Hibiya, T. (2020). A parameterization of local and remote tidal mixing. *Journal of*

Advances in Modeling Earth Systems. doi: 10.1029/2020ms002065

Donners, J., Drijfhout, S. S., & Hazeleger, W. (2005). Water Mass Transformation and Subduction in the South Atlantic. *Journal of Physical Oceanography*, *35*(10), 1841–1860. Retrieved from `http://journals.ametsoc.org/doi/abs/10.1175/JPO2782.1` doi: 10.1175/JPO2782.1

Forget, G., Ferreira, D., & Liang, X. (2015). On the observability of turbulent transport rates by Argo: Supporting evidence from an inversion experiment. *Ocean Science*, *11*(5), 839–853. doi: 10.5194/os-11-839-2015

Fröb, F., Olsen, A., Våge, K., Moore, G. W., Yashayaev, I., Jeansson, E., & Rajasakaren, B. (2016). Irminger Sea deep convection injects oxygen and anthropogenic carbon to the ocean interior. *Nature Communications*, *7*. doi: 10.1038/ncomms13244

Fukumori, I., Wang, O., Fenty, I., Forget, G., Heimbach, P., & Ponte, R. M. (2017). ECCO Version 4 Release 3. *Dspace.Mit.Edu*, *2*(2015), 10. Retrieved from `https://dspace.mit.edu/handle/1721.1/110380{\%}0Ahttp://hdl.handle.net/1721.1/110380` doi: 1721.1/110380

Gaillard, F., Reynaud, T., Thierry, V., Kolodziejczyk, N., & Von Schuckmann, K. (2016). In situ-based reanalysis of the global ocean temperature and salinity with ISAS: Variability of the heat content and steric height. *Journal of Climate*, *29*(4), 1305–1323. doi: 10.1175/JCLI-D-15-0028.1

Garcia, H. E., Weathers, K., Paver, C., Smolyar, I., Boyer, T., Locarnini, R., . . . Reagan, J. (2019). WORLD OCEAN ATLAS 2018 Volume 3: Dissolved Oxygen, Apparent Oxygen Utilization, and Dissolved Oxygen Saturation. *NOAA Atlas NESDIS 83*, *3*(July), 38pp.

Gent, P. R., & McWilliams, James, C. (1990). Isopycnal Mixing in Ocean Circulation Models. *Journal of Physical Oceanography*, *20*, 150–155. doi: 10.1175/1520-0485(1990)020⟨0150:IMIOCM⟩2.0.CO;2

Gruber, N., Gloor, M., Fan, S. M., & Sarmiento, J. L. (2001). Air-sea flux of oxygen estimated from bulk data: Implications for the marine and atmospheric oxygen cycles. *Global Biogeochemical Cycles*, *15*(4), 783–803. doi: 10.1029/2000GB001302

Hanawa, K., & Talley, L. D. (2001). Mode waters. *Ocean Circulation and Climate: Observing and Modeling the Global Ocean*, 373–386 (736pp). Retrieved from `ftp://bslictb.nerc-bas.ac.uk/jbsall/Papers{\_}CMIP5team/2001Hanawa.pdf`

Helm, K. P., Bindoff, N. L., & Church, J. A. (2011). Observed decreases in oxygen content of the global ocean. *Geophysical Research Letters*, *38*(23), 1–6. doi: 10.1029/2011GL049513

Ito, T., Minobe, S., Long, M. C., & Deutsch, C. (2017). Upper ocean O 2 trends: 1958-2015 . *Geophysical Research Letters*, *44*(9), 4214–4223. doi: 10.1002/2017gl073613

Joos, F., Platiner, G. K., Stocker, T. F., Kortzinger, A., & Wallace, D. W. (2003). Trends in marine dissolved oxygen: Implications for ocean circulation changes and the carbon budget. *Eos*, *84*(21), 84–86. doi: 10.1029/2003EO210001

Karstensen, J., Stramma, L., & Visbeck, M. (2008). Oxygen minimum zones in the eastern tropical Atlantic and Pacific oceans. *Progress in Oceanography*, *77*(4), 331–350. doi: 10.1016/j.pocean.2007.05.009

Keeling, R. F., & Garcia, H. E. (2002). The change in oceanic O2 inventory associated with recent global warming. *Proceedings of the National Academy of Sciences of the United States of America*, *99*(12), 7848–7853. doi: 10.1073/pnas.122154899

Keeling, R. F., Körtzinger, A., & Gruber, N. (2010). Ocean Deoxygenation in a Warming World. *Annual Review of Marine Science*, *2*(1), 199–229. Retrieved from `http://www.annualreviews.org/doi/10.1146/annurev.marine.010908.163855` doi: 10.1146/annurev.marine.010908.163855

Klocker, A., & Abernathey, R. (2014). Global patterns of mesoscale eddy properties and diffusivities. *Journal of Physical Oceanography*, *44*(3), 1030–1046. doi: 10.1175/JPO-D-13-0159.1

Koelling, J., Wallace, D. W., Send, U., & Karstensen, J. (2017). Intense oceanic uptake of oxygen during 2014–2015 winter convection in the Labrador Sea. *Geophysical Research*

Letters, *44*(15), 7855–7864. doi: 10.1002/2017GL073933
Köhl, A., Stammer, D., & Cornuelle, B. (2007). Interannual to decadal changes in the ECCO global synthesis. *Journal of Physical Oceanography*, *37*(2), 313–337. doi: 10.1175/JPO3014.1
Kolodziejczyk, N., & Gaillard, F. (2013). Variability of the Heat and Salt Budget in the Subtropical Southeastern Pacific Mixed Layer between 2004 and 2010: Spice Injection Mechanism. *Journal of Physical Oceanography*, *43*(9), 1880–1898. Retrieved from `http://journals.ametsoc.org/doi/abs/10.1175/JPO-D-13-04.1` doi: 10.1175/JPO-D-13-04.1
Kolodziejczyk, N., Llovel, W., & Portela, E. (2019). Interannual variability of upper ocean water masses as inferred from Argo Array. *Journal of Geophysical Research: Oceans*, *i*, 1–19. doi: 10.1029/2018jc014866
Kolodziejczyk, N., Prigent-Mazella, A., & Gaillard, F. (2017). ISAS-15 temperature and salinity gridded fields. *SEANOE*. doi: https://doi.org/10.17882/52367
Körtzinger, A., Schimanski, J., Send, U., & Wallace, D. (2004). The ocean takes a deep breath. *Science*, *306*(5700), 1337. doi: 10.1126/science.1102557
Kwon, E. Y., Deutsch, C., Xie, S. P., Schmidtko, S., & Cho, Y. K. (2016). The North Pacific oxygen uptake rates over the past half century. *Journal of Climate*, *29*(1), 61–76. doi: 10.1175/JCLI-D-14-00157.1
Liu, L. L., & Huang, R. X. (2012). The global subduction/obduction rates: Their interannual and decadal variability. *Journal of Climate*, *25*(4), 1096–1115. doi: 10.1175/2011JCLI4228.1
Long, M. C., Deutsch, C., & Ito, T. (2016). Finding forced trends in oceanic oxygen. *Global Biogeochemical Cycles*, *30*(2), 381–397. doi: 10.1002/2015GB005310
Lumpkin, R., & Speer, K. (2007). Global ocean meridional overturning. *Journal of Physical Oceanography*, *37*(10), 2550–2562. doi: 10.1175/JPO3130.1
Luyten, J., Pedlosky, J., & Stommel, H. (1983). The ventilated thermocline. *Journal of Physical Oceanography*, *13*, 292–309. doi: 10.1007/BF02423489
Luyten, J., Stommel, H., & Wunsch, C. (1985). *A Diagnostic Study of the Northern Atlantic Subpolar Gyre* (Vol. 15) (No. 10). doi: 10.1175/1520-0485(1985)015⟨1344:adsotn⟩2.0.co;2
Marshall, J. (1999). OPEN-OCEAN CONVECTION: OBSERVATIONS, THEORY, AND MODELS. *Reviews of Geophysics*, *37*(1), 1–64.
Marshall, J., & Speer, K. (2012). Closure of the meridional overturning circulation through Southern Ocean upwelling. *Nature Geoscience*, *5*(3), 171–180. Retrieved from `http://dx.doi.org/10.1038/ngeo1391` doi: 10.1038/ngeo1391
Marshall, J., Williams, R. G., & Nurser, A. J. G. (1993). *Inferring the Subduction Rate and Period over the North Atlantic* (Vol. 23) (No. 7). doi: 10.1175/1520-0485(1993)023⟨1315:ITSRAP⟩2.0.CO;2
McCartney, M. S. (1982). *The subtropical recirculation of mode waters* (Vol. 40) (No. Supplement). Retrieved from `http://www.whoi.edu/science/PO/people/mmccartney/pdfs/McCartney82.pdf`
Munk, W., & Wunsch, C. (1998). Abyssal recipes II: Energetics of tidal and wind mixing. *Deep-Sea Research Part I: Oceanographic Research Papers*, *45*(12), 1977–2010. doi: 10.1016/S0967-0637(98)00070-3
Naveira Garabato, A. C., MacGilchrist, G. A., Brown, P. J., Evans, D. G., Meijers, A. J., & Zika, J. D. (2017). High-latitude ocean ventilation and its role in Earth's climate transitions. *Philosophical Transactions of the Royal Society A: Mathematical, Physical and Engineering Sciences*, *375*(2102). doi: 10.1098/rsta.2016.0324
Osborn, T. (1980). Estimates of the local rate of vertical diffusion from dissipation measurements. *Journal of Physical Oceanography*, *10*, 83–89.
Oschlies, A., Brandt, P., Stramma, L., & Schmidtko, S. (2018). Drivers and mechanisms of ocean deoxygenation. *Nature Geoscience*, *11*(7), 467–473. Retrieved from `http://dx.doi.org/10.1038/s41561-018-0152-2` doi: 10.1038/s41561-018-0152-2
Portela, E., Kolodziejczyk, N., Maes, C., & Thierry, V. (2020). Interior water-mass vari-

ability in the Southern Hemisphere oceans during the last decade. *Journal of Physical Oceanography*, *50*(2), 361–381. doi: 10.1175/JPO-D-19-0128.1

Qiu, B., & Huang, R. X. (1995). *Ventilation of the North Atlantic and North Pacific: subduction versus obduction* (Vol. 25) (No. 10).

Rahmstorf, S., Box, J. E., Feulner, G., Mann, M. E., Robinson, A., Rutherford, S., & Schaffernicht, E. J. (2015). Exceptional twentieth-century slowdown in Atlantic Ocean overturning circulation. *Nature Climate Change*, *5*(5), 475–480. doi: 10.1038/nclimate2554

Resplandy, L. (2018). Climate change and oxygen in the ocean. *Nature*, *557*, 314–315. doi: 10.1038/nature15216

Richardson, K., & Bendtsen, J. (2017). Photosynthetic oxygen production in a warmer ocean: The Sargasso Sea as a case study. *Philosophical Transactions of the Royal Society A: Mathematical, Physical and Engineering Sciences*, *375*(2102). doi: 10.1098/rsta.2016.0329

Rintoul, S. R. (2000). Southern Ocean currents and climate. *Papers and Proceedings of the Royal Society of Tasmania*, *133*(3), 41–50. doi: 10.26749/rstpp.133.3.41

Sallée, J. B., Matear, R. J., Rintoul, S. R., & Lenton, A. (2012). Localized subduction of anthropogenic carbon dioxide in the Southern Hemisphere oceans. *Nature Geoscience*, *5*(8), 579–584. Retrieved from `http://dx.doi.org/10.1038/ngeo1523` doi: 10.1038/ngeo1523

Sallée, J.-B., Speer, K., Rintoul, S., & Wijffels, S. (2010). Southern Ocean Thermocline Ventilation. *Journal of Physical Oceanography*, *40*(3), 509–529. Retrieved from `http://journals.ametsoc.org/doi/abs/10.1175/2009JPO4291.1` doi: 10.1175/2009JPO4291.1

Schmidtko, S., Stramma, L., & Visbeck, M. (2017). Decline in global oceanic oxygen content during the past five decades. *Nature*, *542*(7641), 335–339. Retrieved from `http://dx.doi.org/10.1038/nature21399` doi: 10.1038/nature21399

Speer, K., Rintoul, S. R., & Sloyan, B. (2000). The Diabatic Deacon Cell*. *Journal of Physical Oceanography*, *30*(12), 3212–3222. doi: 10.1175/1520-0485(2000)030⟨3212:tddc⟩2.0.co;2

Stramma, L., Johnson, G. C., Sprintall, J., & Mohrholz, V. (2008). Expanding oxygen-minimum zones in the tropical oceans. *Science*, *320*(5876), 655–658. doi: 10.1126/science.1153847

Tuerena, R. E., Williams, R. G., Mahaffey, C., Vic, C., Green, J. A., Naveira-Garabato, A., … Sharples, J. (2019). Internal Tides Drive Nutrient Fluxes Into the Deep Chlorophyll Maximum Over Mid-ocean Ridges. *Global Biogeochemical Cycles*, *33*(8), 995–1009. doi: 10.1029/2019GB006214

Wolf, M. K., Hamme, R. C., Gilbert, D., Yashayaev, I., & Thierry, V. (2018). Oxygen Saturation Surrounding Deep Water Formation Events in the Labrador Sea From Argo-O2 Data. *Global Biogeochemical Cycles*, *32*(4), 635–653. doi: 10.1002/2017GB005829

Wyrtki, K. (1965). Surface Currents of the Eastern Tropical Pacific Ocean. *Inter-American Tropical Tuna Comission*, *9*(5), 271 – 304.

Yeager, S. G., & Large, W. G. (2007). Observational evidence of winter spice injection. *Journal of Physical Oceanography*, *37*(12), 2895–2919. doi: 10.1175/2007JPO3629.1

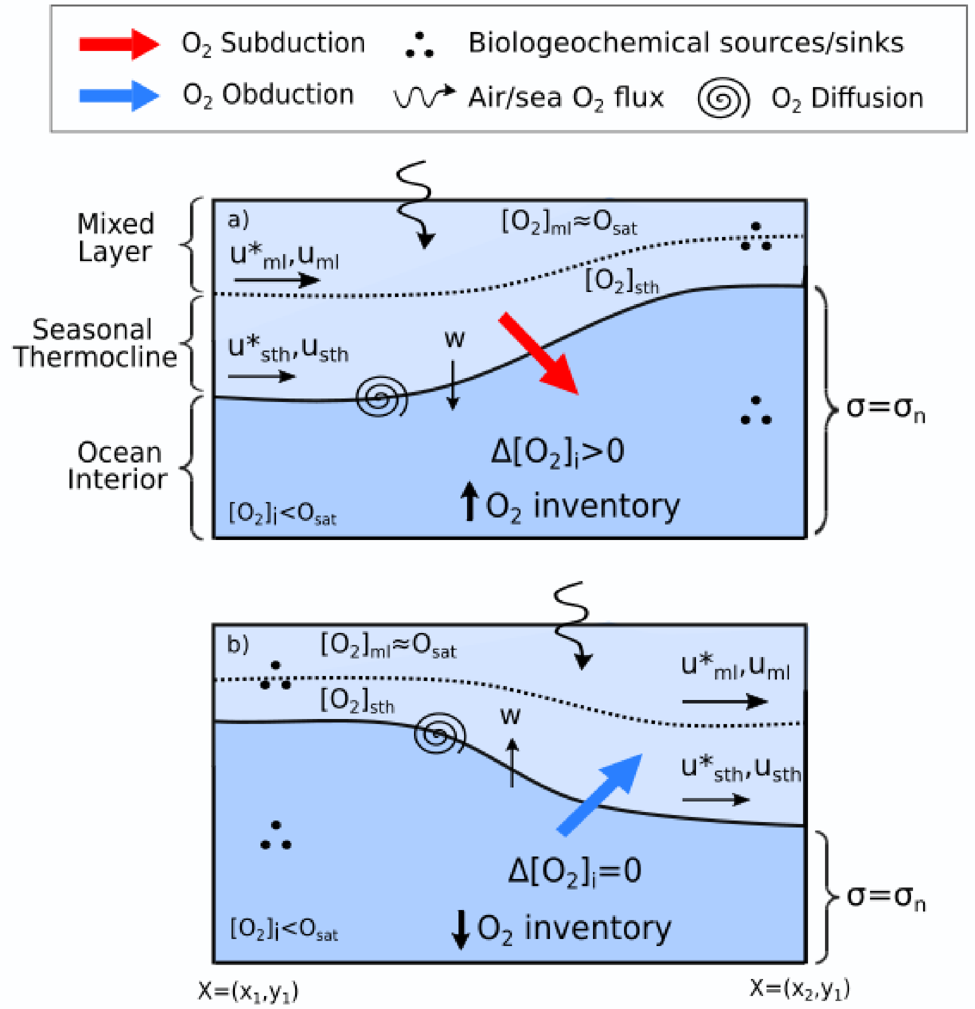

Figure 1. Schematic of the elements implied in a) S^{ox} and b) O^{ox} and their effect on the oxygen inventory and $[O_2]_i$ within a seawater volume confined between the steady late winter ML base and a variable density surface ($\sigma = \sigma_n$). Subduction brings oxygenated waters with $[O_2] \approx O_{sat}$ into the ocean interior which augments the interior oxygen inventory and the $[O_2]_i$. In contrast, obduction reduces the interior oxygen inventory due to the net volume loss, but the $[O_2]_i$ remains invariable. Subduction is computed by taking into account the different geostrophic and eddy velocity within the mixed layer (ml) and the seasonal thermocline (sth). Note that, for clarity, the S^{ox} terms showed in the schematic point in the direction of the net flux, but different combinations are possible

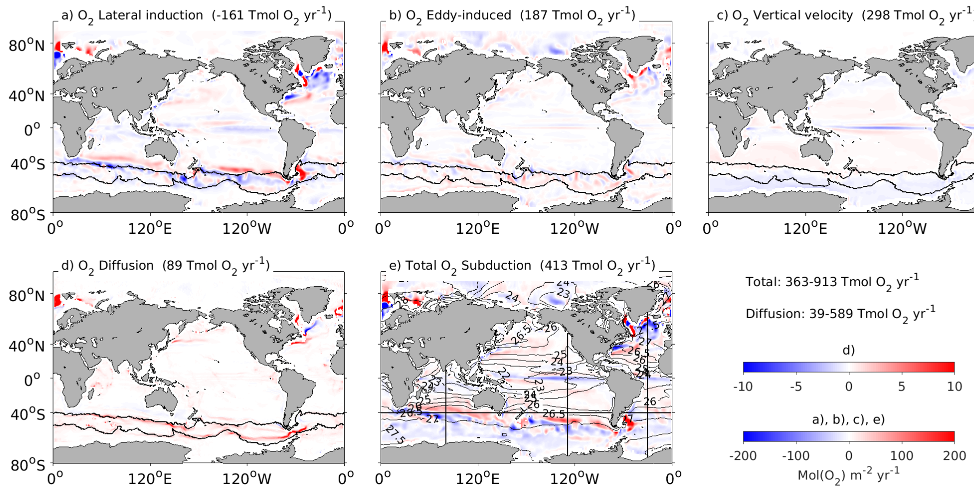

Figure 2. Spatial distribution of the S^{ox} and its component terms. a) Lateral induction, b) eddy-induced, c) vertical velocity d) oxygen diffusion and e) Total S^{ox}. Note the different scale in d) which is one order of magnitude smaller than the other terms. Contours in (a-d) indicate the average limits of the ACC. Contours in (e) are the isopycnals at the deepest ML base. The straight lines in (e) indicate the position of the sections plotted in Figure 3. The globally integrated contribution of each term is indicated on panel's titles and the two extremes for diffusion and the total oxygen flux are shown on top of the colorbars

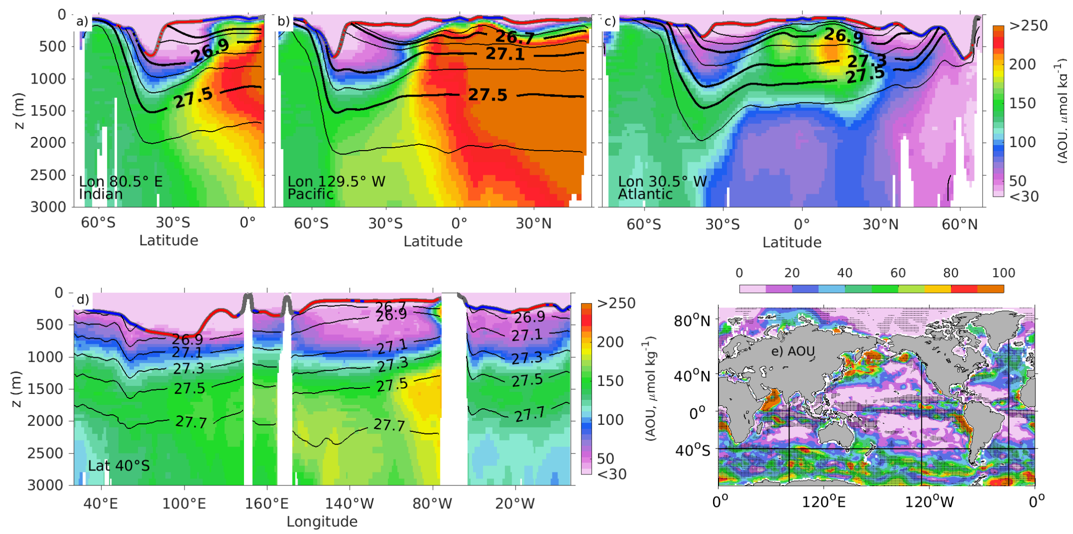

Figure 3. a-c) Mean meridional sections of AOU across the a) Indian b) Pacific and c) Atlantic oceans. d) Zonal section of AOU at 40°S. Black contours in a-d represent the mean position of the isopycnals from 26.5 kg m^{-3} to 27.7 kg m^{-3} and the thicker lines illustrate the SAMW and AAIW limits in every basin. The thick grey contour represent the deepest ML depth which has blue and red dots superimposed to indicate the subduction and obduction zones respectively. e) AOU at the late winter ML base. The stippling corresponds with obductive regions. The straight lines in e) represent the position of the sections.

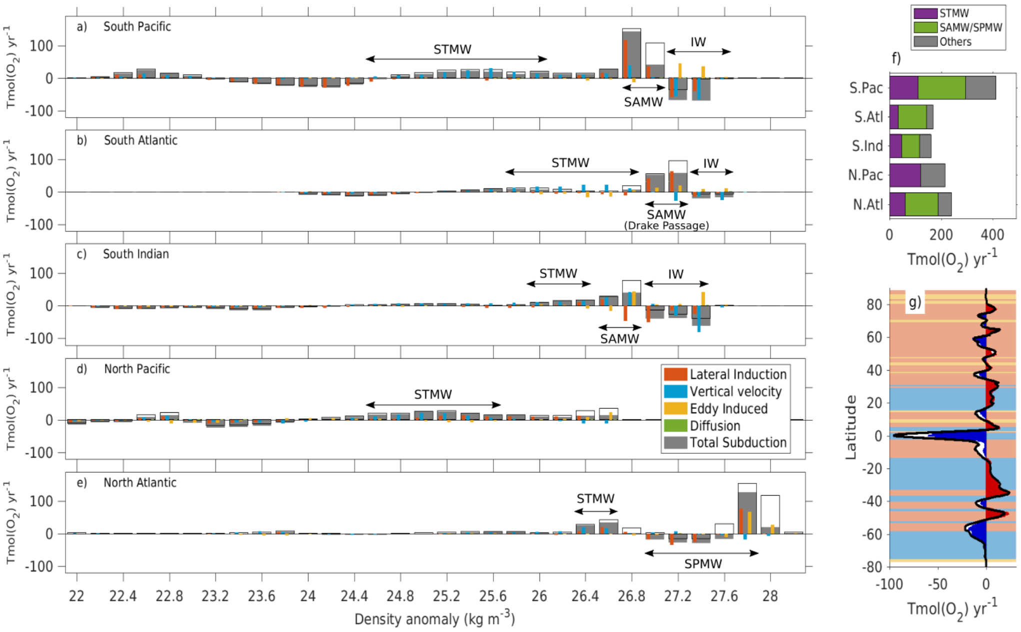

Figure 4. (a-e) Mean oxygen subduction rates and the contribution of each term by density class. The bars contour represent the total S^{ox} with the maximum oxygen diffusion f) Contribution of the STMW and SA-SPMW to the total oxygen uptake in each basin. g) Zonal average of kinematic oxygen subduction rates where red (blue) colors indicate net S^{ox} (O^{ox}). The solid black curve represents the zonal oxygen flux assuming an homogeneous spatial oxygen distribution (global average value). This curve demonstrates the small role that the $[O_2]$ distribution plays on the total S^{ox}. The background shading in g) shows the zonally dominant subduction component. The shading colors correspond to the legend in panel d)